Journal of Non-Crystalline Solids 613 (2023) 122373

Contents lists available at ScienceDirect

Journal of Non-Crystalline Solids

journal homepage: www.elsevier.com/locate/jnoncrysol

Magnetic properties evaluation of Fe-based amorphous alloys synthesized via spark plasma sintering

D.W. Zhang [a,b,1], Y. Zhang [b,c,1,*], Y.F. Cai [b], B.W. Zang [b], F. Zhao [d], Y.C. Wang [e], R. Umetsu [f], Z.Z. Li [g], X. Tong [h], J.T. Huo [b,c], S.L. Che [a,*], J.Q. Wang [b,c,*]

[a] School of Materials Science and Engineering, Zhejiang University of Technology, Hangzhou 310014, China
[b] CAS Key Laboratory Science of Magnetic Materials and Devices, and Zhejiang Province Key Laboratory of Magnetic Materials and Application Technology, Ningbo Institute of Materials Technology and Engineering, Chinese Academy of Science, Ningbo 315201, China
[c] Center of Materials Science and Optoelectronics Engineering, University of Chinese Academy of Sciences, Beijing 100049, China
[d] TIZ Advanced Alloy Technology Co., Ltd., Quanzhou 362000, China
[e] School of Physical Science and Technology, Northwestern Polytechnical University, Xi'an 710072, China
[f] Institute for Material Research, Tohoku University, Sendai 980-8577, Japan
[g] Jiangsu JITRI Advanced Energy Materials Research Institute Co., Ltd., Changzhou 213000, China
[h] Songshan Lake Materials Laboratory, Dongguan 523808, China

ARTICLE INFO

Keywords:
Powder compact
Amorphous
Spark plasma sintering (SPS)
Magnetic flux density (*B*)

ABSTRACT

$Fe_{77.7}Si_8B_{10}P_4Cu_{0.3}$ amorphous powder compacts with high relative density ($\rho_r = 94\%$), high saturated magnetic induction ($B_s = 1.34$ T), and high permeability ($\mu = 163$ at 20 kHz) were fabricated by spark plasma sintering. In this work, $Fe_{77.7}Si_8B_{10}P_4Cu_{0.3}$ spherical amorphous powders with good amorphous forming ability were prepared by regulating the material composition and the particle size distribution by gas atomization at first. The effect of sintering temperature (T_s) on the structure and magnetic properties of powder compacts was systematically investigated. The powder compacts sintered at T_s of 696–712 K were found to remain amorphous structure and exhibit optimal structural and magnetic performance, due to the high temperature and high pressure employed in SPS with high heating rate. These results are promising for the applications of Fe-based amorphous powder alloys in soft magnetic devices requiring tens of kilo-hertz frequency.

Introduction

Since the second industrial revolution, soft magnetic materials have been widely used in electronic devices for power generation and distribution [1]. Non-oriented electrical steel is still dominating the market owing to its excellent saturated magnetic flux density (B_s) and inexpensive process costs [2]. However, electrical steel cannot easily adapt to the high-frequency electronic devices in the 5G era due to its extremely high core loss (*W*) [3–5]. Soft magnetic ferrites have very low core loss in high frequency applications owing to their low electrical conductivity [6]. However, the applications of soft magnetic ferrites are limited because of its low B_s (below 0.5 T) [7].

Fe-based amorphous alloys characterized by the disordered atomic arrangements have high permeability (μ) and low *W*. Their disordered atomic arrangements reduces the mean free path of electrons and hence resulting in a 2 to 3-fold higher resistivity than the crystalline alloys, which helps reduce the eddy current loss. In addition, a high concentration of Fe would result in a high B_s. Therefore, Fe-based amorphous alloys have received increasing attention as an alternative material to traditional silicon steel and soft ferrites [8–13].

Mass-produced high B_s Fe-based amorphous materials are often in thin ribbons prepared by the melt spinning process due to the undesirable amorphous-forming ability (AFA). However, the machinability of thin ribbons is challenging, which cannot meet the application requirements and the shape conformations of electronic devices [14,15]. It can be addressed through the preparation of Fe-based amorphous alloy powders in powder compacts by powder metallurgy processes [16–19]. Fe-based amorphous alloy powders practically used in powder metallurgy processes mainly include (i) flake powders obtained by mechanical crushing [20] or ball milling [21] and (ii) spherical powders

* Corresponding author.
E-mail addresses: yzhang@nimte.ac.cn (Y. Zhang), cheshenglei@zjut.edu.cn (S.L. Che), jqwang@nimte.ac.cn (J.Q. Wang).
[1] These authors contributed equally to this work.

https://doi.org/10.1016/j.jnoncrysol.2023.122373
Received 16 February 2023; Received in revised form 22 April 2023; Accepted 29 April 2023
Available online 6 May 2023

manufactured by atomization [22]. Among these, powder compacts prepared from flake powders are typically characterized by high density and saturated magnetic flux density. However, the orientation of flakes often occurs during the pressing process, resulting in anisotropy of the bulk sample [23,24]. This phenomenon can be prevented by using spherical powders due to the isotropic particle shape [25]. Additionally, the application of spherical powders is also challenging. The atomization preparation process of spherical powders places high demands on the AFA of the alloy and the three-dimensional isotropy of the spherical powders makes it difficult to be fully compacted [26,27]. Previous works have overcome these challenges by regulating material composition with good AFA and improving the powder compacting processes. Zhao et al. [28] prepared gas atomization amorphous alloy powders by partially replacing Si in the FeSiBNbCu composition system with P to improve the AFA. Huang et al. [29] enhanced the density of powder compacts made of spherical powders by using a warm pressing process. This was achieved by using high temperature to soften the magnetic powders and the surface insulation layer, which allows the powder to move easily and fill the pores.

Based on the above ideas, we investigated new pressing processes and composition design methods. The spark plasma sintering (SPS) process is useful for rapid heating and sintering of samples under direct current pulses. The fast heating and cooling during SPS can inhibit the crystallization of amorphous powders [19,30–32]. Meanwhile, the high temperature and high pressure employed in SPS can effectively enhance the density of powder compacts [33,34]. Atomized spherical amorphous powders can be prepared by improving the AFA of powders via reducing the concentration of iron, which is negatively correlated to the AFA, and by increasing the proportion of amorphous-forming elements (B, P) [35,36]. Based on this scheme and the overall goal of preparing powder compacts with high B_s, the Fe-Si-B-P-Cu alloy system with high B_s and abundant amorphous-forming elements has been reported to be suitable [37,38].

Herein, Fe-Si-B-P-Cu spherical powders were prepared by gas atomization process. By modulating the composition and particle size to improve the AFA, spherical powders with an amorphous structure were obtained. A series of bulk amorphous powder compacts were then prepared by the SPS process. The magnetic properties and structures of the resulting compacts were regulated according to the sintering temperature. The results revealed high relative density and saturated magnetic flux density for the powder compacts prepared by SPS.

2. Experimental

2.1. Sample preparation

Alloy ingots ($Fe_{77.7}Si_8B_{10}P_4Cu_{0.3}$, $Fe_{79.7}Si_8B_9P_3Cu_{0.3}$, and $Fe_{81.7}Si_9B_7P_2Cu_{0.3}$), with nominal compositions, were prepared by high-frequency induction melting technique. Briefly, a mixture of high-purity metals (99.9 mass% pure Fe and Cu), metalloids (99.9 mass% Si and 99.5 mass% B), and pre-melted Fe_3P (99.9 mass%) was melted under high-purity argon gas atmosphere after evacuation at a pressure of up to 10^{-3} Pa. Metallic magnetic powders with a particle size of up to 75 μm were prepared by gas atomization. To this end, three kinds of powders with different average particle sizes of ~20, 20~38, and 38~75 μm were obtained after sieving. Disk shape magnetic powder cores (diameter of 12 mm) were compacted by a spark plasma sintering machine (DR..SINTER(R) SPS-3.20MK-IV machine) consisting of a pressure system with two tungsten carbide press bars and a sintering system for providing a vacuum environment and rapid heating. The coated powders were then applied at a molding pressure of 800 MPa from room temperature to the sintered temperature (T_s, 636–783 K) under vacuum at a heating rate of 100 K/min. After reaching the T_s, the heating process was stopped abruptly, with almost zero holding time and the sample was left to naturally cool to room temperature. The sintering pressure was released at a sample temperature below 573 K. The obtained toroidal powder alloy compact was processed and transformed from a disk shape to a toroidal shape by a perforation process, with an out diameter of 12 mm and an inner diameter of 8 mm.

2.2. Characterization

The thermal stability and phase transformation temperatures were studied by differential scanning calorimetry (DSC, NETZSCH 404C). The nano-crystallization behavior of the as-quenched and bulk cores sintered at different sintering temperatures (T_s) was explored by X-ray diffraction (XRD, Bruker D8 Advance) with Cu Kα radiation. The magnetic permeability (μ) was measured by a precision impedance analyzer (Agilent 4294A). The saturation magnetization (M_s) was determined by a vibrating sample magnetometer (VSM, Lakeshore7410) under a maximum magnetic field of 800 kA/m. The saturated magnetic flux density (B_s) was calculated by the formula:

$$B_s = \frac{4\pi\rho M_s}{10^4}$$

The coercivity (H_c) of each toroidal compact sample was measured by a Rikken Denshi DC B-H loop tracer with a maximum magnetic field of 8 kA/m. The core loss (W) was estimated using an AC B-H analyzer (Linkjoin MATS-2010SA). The density was determined by measuring the weight and physical volume of each compact sample.

3. Results and discussion

The amorphous powders were first screened by customized modulation of composition and particle size. In Fig. 1, the phase structure identification and evaluation of the AFA of $Fe_{81.7}Si_9B_7P_2Cu_{0.3}$, $Fe_{79.7}Si_8B_9P_3Cu_{0.3}$, and $Fe_{77.7}Si_8B_{10}P_4Cu_{0.3}$ were given as a function of atomized powder with gradient particle size. Since no significant glass transition temperature (T_g) was found, the AFA is evaluated by analyzing the degree of crystallization of the powder. In all the curves shown in Fig. 1(a), two sharp and tall diffraction peaks were observed at 2θ around 45.6 and 65.7°, while an inconspicuous diffraction peak was seen at 43.0°. The two sharp peaks correspond to the α-Fe(Si) solid solution phase, and the inconspicuous peak can be assigned to the Fe(B,P) compound phase according to the PDF card. In the DSC curve of the $Fe_{81.7}Si_9B_7P_2Cu_{0.3}$ sample (Fig. 1(b)), only one exothermic peak was present at the crystallization temperature (T_x) of about 828 K in all three curves. Additionally, the peak area decreased as a function of the particle size. DSC and XRD data indicated a completely precipitated α-Fe(Si) solid solution phase with the presence of small amounts of Fe(B,P) phase precipitation in all particle-sized $Fe_{81.7}Si_9B_7P_2Cu_{0.3}$ powder samples. This is the result of high Fe and low B and P concentration. It is generally believed that Fe in the material system tends to deteriorate the AFA, while B and P promote it [35,36].

$Fe_{79.7}Si_8B_9P_3Cu_{0.3}$ powders was obtained by partial replacement of Fe by B and P. As shown by the XRD patterns (Fig. 1(c-d)), the characteristic peaks corresponding to α-Fe(Si) solid solution and Fe(B,P) compound are still present. However, they show lower intensity compared with the $Fe_{81.7}Si_9B_7P_2Cu_{0.3}$ powders. The diffuse scattering peak which is typical for amorphous phase is observed near 45° in samples of size 20~38 μm and ~20 μm and can be used as evidence for AFA improvement. The presence of a new exothermic peak at $T_{x1} \approx 778$ K and the increase in the enthalpy of the exothermic peak at $T_{x2} \approx 832$ K reflects less crystallinity of the as-quenched powders. This also reflects an improvement in AFA. Although the powders are still not fully amorphous, it has been proved that it is feasible to further enhance the AFA of Fe-Si-B-P-C powders via replacing Fe by B and P.

The desirable phase structure was determined from the phase structure characterization of the $Fe_{77.7}Si_8B_{10}P_4Cu_{0.3}$ powders (Fig. 1(e-f)). From the XRD patterns in Fig. 1(e), a clear diffuse scattering peak, typical for an Fe-based amorphous material can be observed between 2θ of 40–50°. Two overlapping and exothermic peaks ($T_{x1} \approx 795$ K, $T_{x2} \approx$

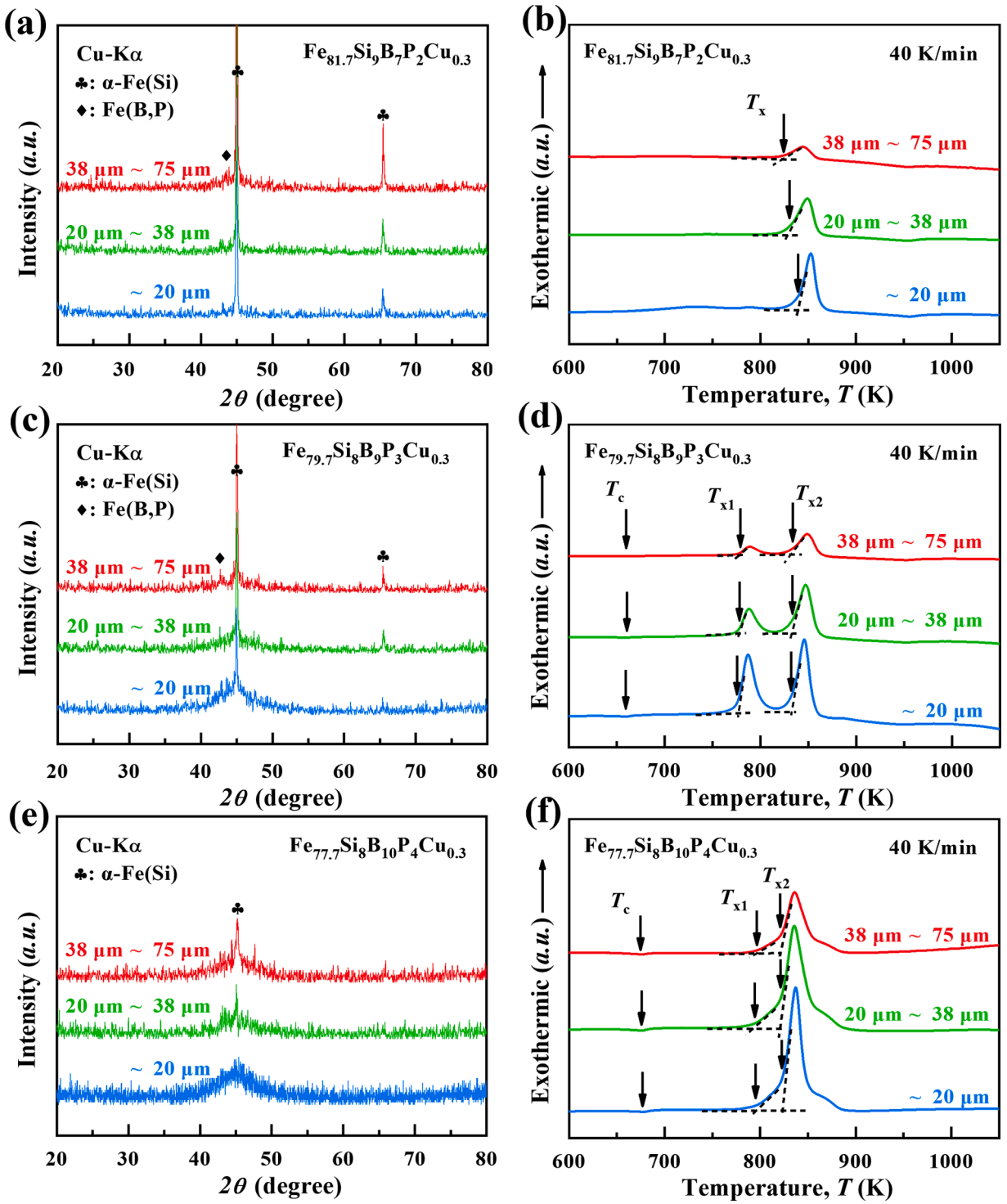

Fig. 1. XRD patterns of powders (a) $Fe_{81.7}Si_9B_7P_2Cu_{0.3}$, (c) $Fe_{79.7}Si_8B_9P_3Cu_{0.3}$, and (e) $Fe_{77.7}Si_8B_{10}P_4Cu_{0.3}$ with gradient particle size. DSC curves of powders (b) $Fe_{81.7}Si_9B_7P_2Cu_{0.3}$, (d) $Fe_{79.7}Si_8B_9P_3Cu_{0.3}$, and (f) $Fe_{77.7}Si_8B_{10}P_4Cu_{0.3}$ with gradient particle size.

823 K) can be seen in the DSC curves (Fig. 1(f)). These results imply that $Fe_{77.7}Si_8B_{10}P_4Cu_{0.3}$ exhibited a higher AFA than the other two compositions. Typical diffuse scattering peaks were visible in the XRD pattern of the samples (~20 μm), which can be corroborated by the large exothermic peak area in the DSC curve and overlapped two exothermic peaks. Therefore, the $Fe_{77.7}Si_8B_{10}P_4Cu_{0.3}$ powder with an average particle size below 20 μm was identified as the optimal powder for subsequent SPS sintering experiments.

The powder compact sintered at different T_s were further explored by DSC and XRD to identify the crystallization and phase structure. The as-quenched powders were also characterized for phase structure and used as a control group (Fig. 2). The DSC curves in Fig. 2(a) revealed two partially overlapping exothermic peaks in the as-quenched powder. For sintered samples, the peak areas did not change significantly as a function of the sintering temperature below 712 K. As the T_s increased, the DSC curves showed significant changes. For instance, the bulge on the right side of the main exothermic peak disappeared rapidly at T_s above 725 K, while all the exothermic peaks vanished at T_s up to 783 K.

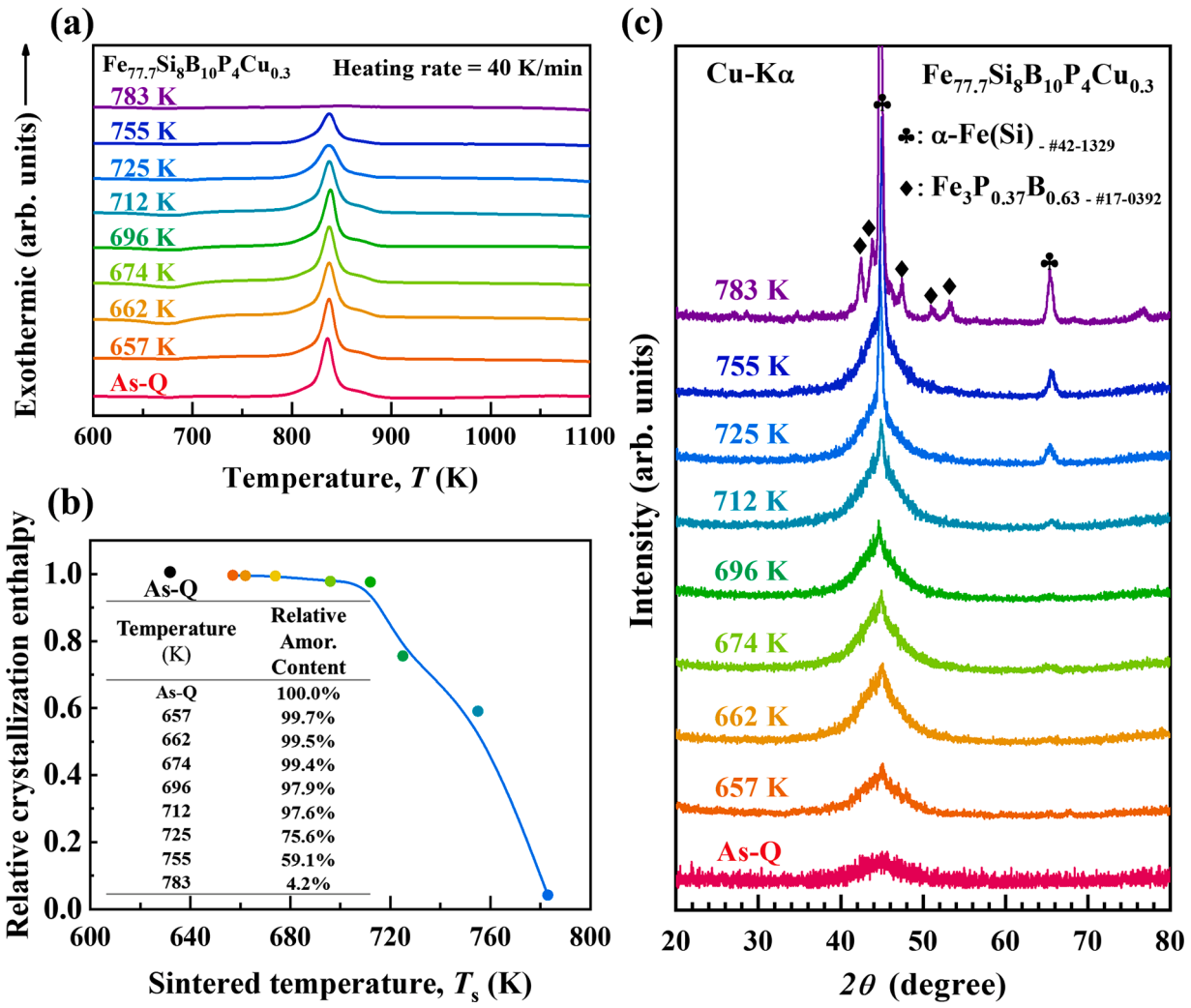

Fig. 2. (a) DSC curves, (b) relative crystallization enthalpy and (c) XRD patterns of bulk $Fe_{77.7}Si_8B_{10}P_4Cu_{0.3}$ powder cores sintered at different temperatures.

Although the T_s chosen were lower than the T_{x1} of $Fe_{77.7}Si_8B_{10}P_4Cu_{0.3}$, obvious crystallization was observed in powder compacts with T_s above 725 K. The T_s in the experiments was measured by a thermocouple inside the mold. On the one hand, there is a temperature difference between the thermocouple and the powders. On the other hand, the transient high temperature field generated between the powders by pulsed energy and Joule heating makes the actual temperature of the powders higher than the set point [39]. The degrees of crystallization of the samples sintered at different T_s were quantitatively characterized by determining the relative enthalpy of crystallization by calculating the area of the exothermic peak [40]. In Fig. 2(b), the enthalpy of crystallization of the as-quenched powder was considered 100% and used to estimate the percentage of crystallization enthalpy for each T_s. Below 712 K, the enthalpy of crystallization did not change significantly. At sintering temperatures above 712 K, the enthalpy of crystallization of the sintered samples decreased rapidly. At temperatures reaching 783 K, the enthalpy of crystallization declined to 4.2%. The change in the relative crystallization enthalpy indicates that the rapid sintering process of SPS does not lead to obvious crystallization of the sample when the T_s is below 712 K. Therefore, it is appropriate to sinter below 712 K for the preparation of amorphous powder compacts.

The changes of crystallization diffraction peak in XRD patterns (Fig. 2(c)) are consistent with the variations in the area and crystallization enthalpy of exothermic peak in DSC curves. At T_s between 662 and 712 K, the XRD curves of all the sintered compact samples showed basic diffuse scattering peaks like the as quenched powder sample. Small crystallization peaks observed in this temperature band are the precipitation of tiny grains on the amorphous matrix. Towering and sharp crystallization peaks of the α-Fe(Si) solid solution and Fe(B,P) compound phases were found in samples sintered up to 725 K and above. This corresponds to significant changes in the exothermic DSC peaks of samples sintered at temperatures greater than or equal to 725 K. The other phases especially the Fe(B,P) compound phase, precipitated at T_s of up to 783 K can worsen the magnetic properties of the sample [41,42]. Since the samples sintered at 783 K were almost completely crystallized and did not meet the needs of this work, the magnetic properties of the samples sintered at this temperature were not characterized subsequently.

Density is a key parameter in the pressing process and greatly affects the magnetic properties of the powder compact. The trend of the density of the powder compacts prepared by SPS with T_s is shown in Fig. 3. The density of the powder compacts increases in an S-shape with the increase of T_s. At T_s below 712 K, the density increase is mainly due to the increased plasticity which makes the powders more easily to be compacted [43]. The increase in density with T_s above 712 K comes from the disorder-order transition on the one hand [44]. On the other hand, large-sized grains precipitated at high T_s exhibit lower hardness and good plasticity, which makes the powders more compactible.

To identify the optimal T_s to obtain excellent soft magnetic properties, the density and magnetic properties of powder compacts obtained at different T_s were examined. The critical parameters related to relative density, saturated magnetic flux density, and coercivity were first

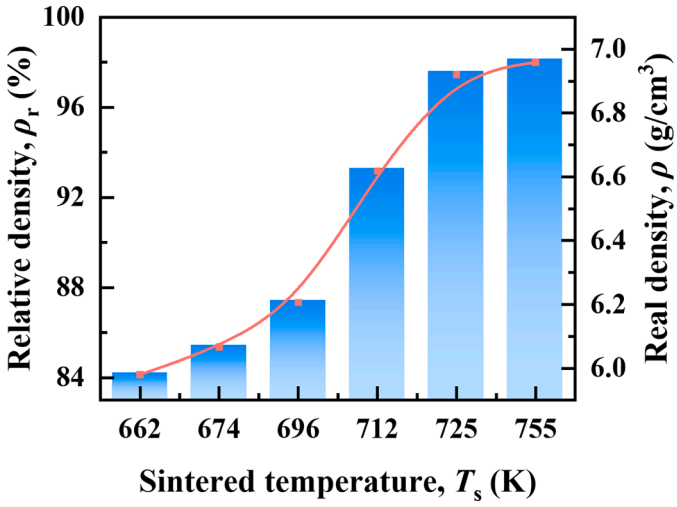

Fig. 3. Relative and true densities of powder compacts prepared at different T_s.

studied and the results are shown in Fig. 4. The saturated magnetic flux density of the $Fe_{77.7}Si_8B_{10}P_4Cu_{0.3}$ amorphous powder compacts measured by VSM revealed high M_s (above 150 emu/g) at each sintering temperature. By increasing T_s from 662 to 712 K, the M_s gradually increased from 148 to 161.8 emu/g. Subsequently, M_s slowly decreases to 154.1 emu/g when T_s further increases up to 755 K. The slight increase of M_s with higher annealing temperature could be attributed to the progress of α-Fe crystallization and the improved short or medium range ordering in the amorphous matrix. This phenomenon is consistent with the work of other researcher, may be related to the densification [45]. The decrease in M_s with increasing T_s above 712 K is mainly due to the grain growth and precipitation of Fe(B,P) compounds, which are widely believed to deteriorate M_s [46].

In Fig. 4(b), the effect of T_s change on H_c reveals a valley-shaped profile. At T_s below 712 K, H_c decreased from 2.73 to 2.26 Oe as T_s increases. It increases to 3.4 Oe rapidly when T_s further rises from 712 to 755 K. It is well known that H_c is very sensitive to the structural defects. It includes crystal defects such as dislocation at micro scale and pinning structures such as pores at macro scale. Amorphous has very small structure correlation length due to its long-range disorder [47,48]. Smaller structure correlation length means smaller magnetic exchange length, and smaller magnetic exchange length mean fewer staples such as dislocation in the magnetization process and resulting in lower H_c. Boosting the density can reduces porosity can be reduced effectively by boosting the density. It allows H_c decreases by reducing the obstruction of the magnetization process. The XRD patterns (Fig. 2(c)) of the sintered samples showed basic amorphous structures and trace nano-crystals when T_s was below 712 K. The structure correlation length remains at lower level at the sintering temperature interval, and the decrease in H_c mainly from the increase in density. When T_s is higher than 712 K, crystals precipitate and grow significantly. The increase in grain size results in a significant increase in structure correlation length and therefore a rapid increase in H_c.

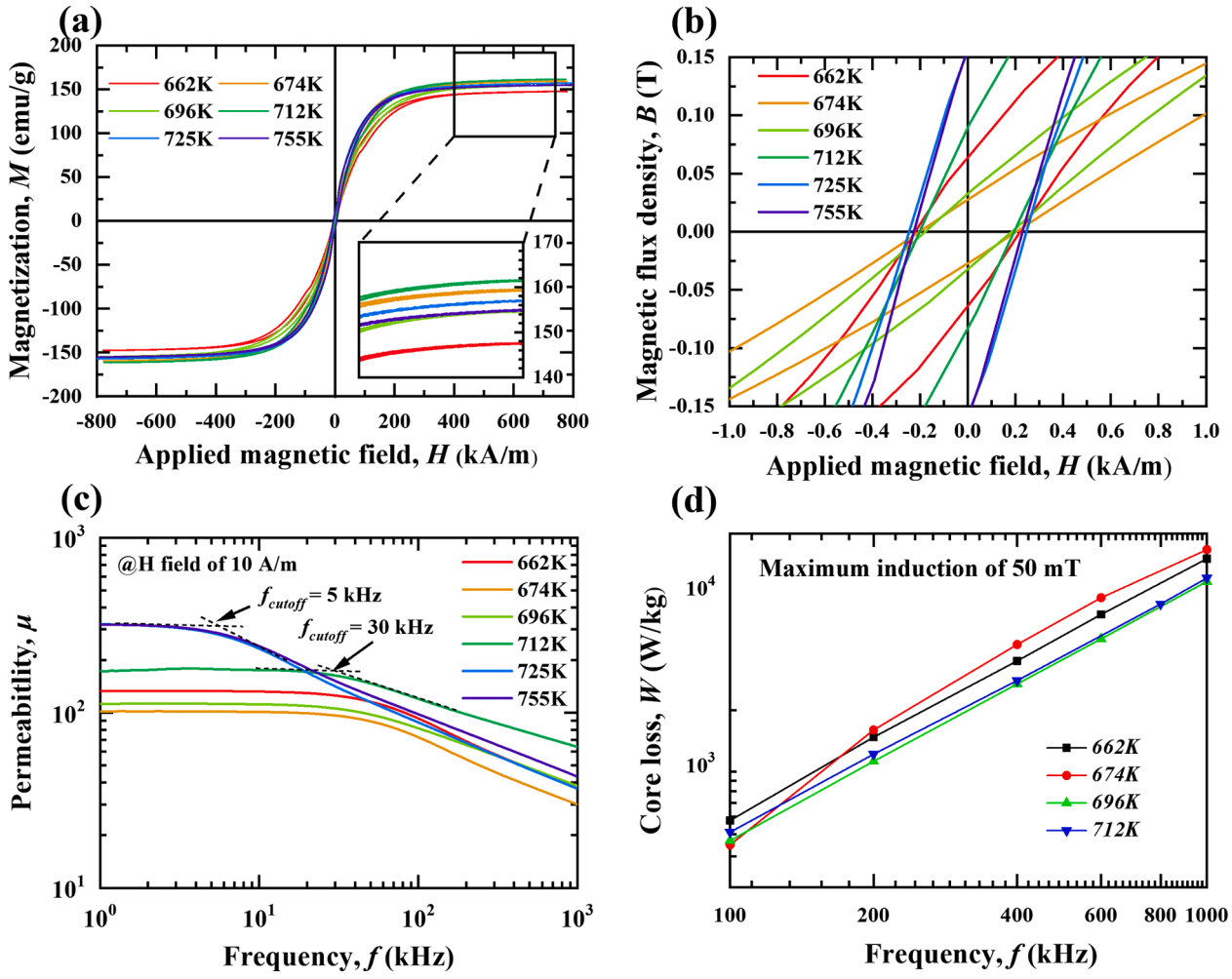

Fig. 4. (a) M_s, (b) H_c, (c) μ, and (d) W of powder compacts prepared at different sintering temperatures.

The permeability of powder compacts was measured in the frequency range of 1 to 1000 kHz at 10 A/m applied field. The results are shown in Fig. 4(c). In the low frequency band below 5 kHz, T_s is basically positively correlated with μ. In this frequency band, the powder compacts with T_s of 725 and 755 K exhibit excellent permeability above 200. The reason for this result is also due to the increased density. Fewer pores and pegs allow a smoother magnetization process, resulting in a higher μ. However, the high μ of the powder compacts with T_s of 725 and 755 K is unstable. Rapid drops of μ can be seen when the frequency is increased to above 10 kHz and the cut-off frequency of the permeability is determined to be only 5 kHz. In contrast, the powder compacts with a T_s of 715 K exhibit both good permeability (163 in about 20 kHz) and good frequency stability (the cutoff frequency was determined to be 30 kHz). The main reason for the difference in frequency stability is difference in resistivity of crystalline and amorphous phases. Low resistivity of the crystals causes more eddy currents at high frequency. Eddy currents act as an inverse magnetic field making magnetization more difficult and thus reducing permeability [49]. Amorphous phase is generally considered to have a higher resistivity, which effectively limits high frequency eddy currents and allows for better stability of magnetic permeability at high frequencies.

The abovementioned differences in resistivity also lead to differences in core loss of the powder compacts with different T_s. The core loss of the powder compacts with amorphous structure ($T_s \leq 712$ K) are characterized in Fig. 4(d). It can be seen that powder compacts with higher sintering temperatures exhibit lower core loss. This is attributed to the further increase in resistivity due to the precipitation of small amount of nano-crystalline grains on one hand. The gradual decrease of the coercivity in this sintering temperature range also leads to a decrease of the hysteresis loss. It is worth mentioning that the powder used in this work is uninsulated and uncoated since the purpose of this study is to develop powder compacts with high ρ and high B_s. It is expected that a lower loss powder can be obtained after insulation coating.

To identify the optimal SPS temperature, the trends of density and magnetic properties with sintering temperature are summarized in Fig. 5. In terms of density, it increases monotonically with increasing sintering temperature. Higher T_s brings better pressing effect. The B_s increases rapidly with increasing T_s at below 712 K causes by increase of density and M_s, and stable at T_s above 712 K because of increase of density and decrease of M_s.

High density reduces the pores between powders and improves the soft magnetic coupling effect between magnetic particles, thus minimizing the H_c when T_s between 696 and 712 K. Powder compacts sintered at 712 K with dense and amorphous structure have good frequency stability of permeability and achieve the highest permeability at 20 kHz. Combining all properties, the optimal T_s parameters can be determined to be between 696 and 712 K.

The density and magnetic properties of the powder compacts with a sintering temperature of 712 K were compared with other related studies, and the results are shown in Table 1. Compared to the cold pressing (CP) process, the powder compacts prepared in this work shows relatively higher ρ_r, B_s, and μ. This indicates that the SPS process has unique advantages in preparing powder compacts with high structural density and high magnetic flux density. Compared with other works using the SPS process, the samples prepared in the present work have high intermediate frequency permeability, but no significant advantage in terms of structural density and magnetic flux density. This may be caused by the lack of excellent intrinsic magnetic properties of the amorphous powders prepared in this work and the lack of tuning of other process parameters. To address this issue, the optimization and improvement will be continued in the next work.

4. Conclusions

$Fe_{77.7}Si_8B_{10}P_4Cu_{0.3}$ amorphous powder compacts were successfully prepared using the SPS process. Following conclusions were drawn:

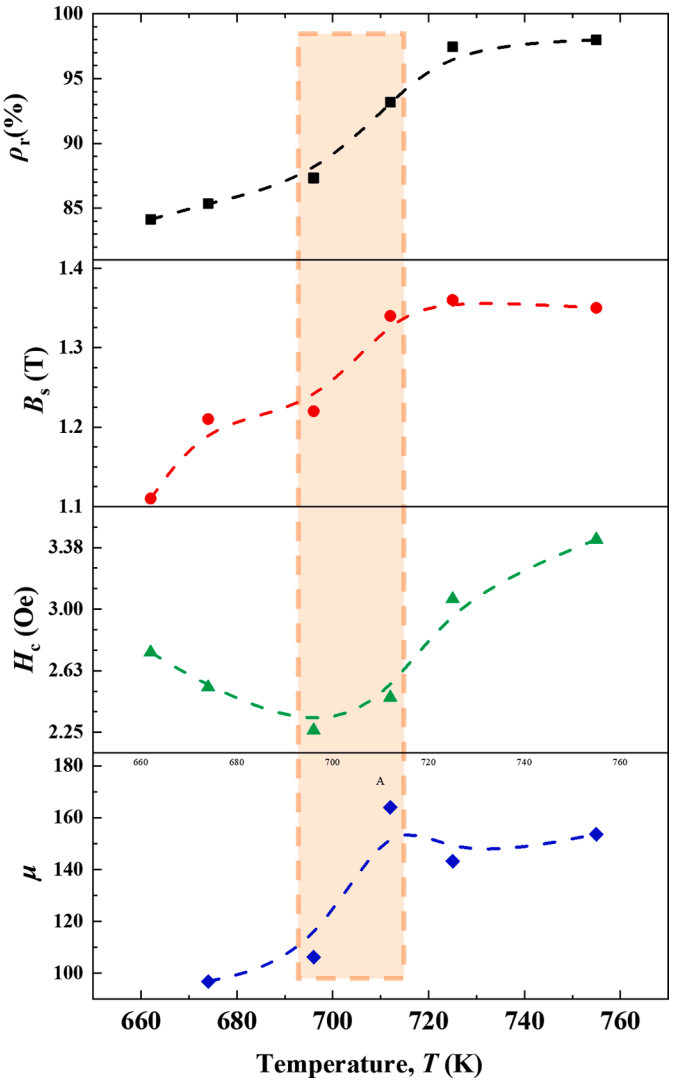

Fig. 5. The trends of density and magnetic properties with sintering temperature.

1 Gas-atomized $Fe_{77.7}Si_8B_{10}P_4Cu_{0.3}$ spherical powders with amorphous structure were successfully prepared by modulating the element concentration (Fe, B, P) and particle size.
2 Dense powder compacts of $Fe_{77.7}Si_8B_{10}P_4Cu_{0.3}$ with good amorphous structure can be prepared when the sintering temperature is below 712 K, due to the high temperature and high pressure employed in SPS with high heating rate.
3 Powder compacts with sintering temperatures of 696–712 K exhibit excellent structure and magnetic performance such as high relative density (94%), high B_s (1.34 T), low H_c (2.3 Oe), and stable μ (163 up to 20 kHz).

Powder compacts fabricated by spark plasma sintering in this work can be expected to apply to soft magnetic devices requiring tens of kilohertz frequency.

CRediT authorship contribution statement

D.W. Zhang: Data curation, Writing – original draft. **Y. Zhang:** Data curation, Conceptualization, Methodology, Writing – review & editing. **Y.F. Cai:** Conceptualization, Methodology, Writing – review & editing. **B.W. Zang:** Data curation, Writing – review & editing. **F. Zhao:** Conceptualization, Methodology. **Y.C. Wang:** Conceptualization,

Table 1
Comparison on the performance of the powder compacts prepared in this work with existing work.

Process	Materials	ρ (g/cm^3)	ρ_r (%)	M_s (emu/g)	B_s (T)	μ	H_c (Oe)	Refs.
SPS	**$Fe_{77.7}Si_8B_{10}P_4Cu_{0.3}$**	**6.67**	**94%**	**163**	**1.34**	**163**	**2.3**	**This work**
	$Fe_{76}Si_{9.6}B_{8.4}P_6$	/	97.60%	/	1.44	/	/	[19]
	$Fe_{48}Cr_{15}Mo_{14}Y_2C_{15}B_6$	/	94.13%	/	/	/	/	[31]
	Fe-Si	6.93	95.59%	169.98	1.43	110	23.15	[50]
	Fe-Si-B	/	/	146.1	/	/	113.4	[51]
	Fe-Si-B-Cu	/	/	159.6	/	/	87	[51]
	Fe-Si-B-Nb	/	/	150.8	/	/	62.4	[51]
	Fe-Si-B-Nb-Cu	/	/	166.8	/	/	109.2	[51]
	$Fe_{84.3}Si_4B_8P_3Cu_{0.7}$	6.25	83.70%	/	/	135	3.75	[52]
	$Fe_{83.3}Si_4B_8P_4Cu_{0.7}$	5.62	89%	/	/	50	2.3	[49]
CP	$Fe_{73.5}Si_{15.5}B_7Cu_1Nb_3$	5.34	75.20%	/	/	84	/	[53]
	$Fe_{73}Si_{13}B_2Cu_1Nb_6$	/	/	135.6	/	49	0.18	[54]
	$Fe_{73.5}Si_{13.5}B_9Nb_3Cu_1$	/	/	/	1.14	80	/	[55]
	Fe-Si-B-C—Cr	/	/	/	/	74	/	[56]
	$(Fe_{0.76}Si_{0.09}B_{0.1}P_{0.05})_{98.5}Nb_1Cu_{0.5}$	5.38	75.92%	155	1.04	85	/	[57]
	$Fe_{73.5}Cu_1Nb_3Si_{15.5}B_7$	6.186	87.07%	125	0.97	115	6	[58]
	$Fe_{77}Si_4B_{10}P_6Nb_2Cr_1$	5.83	/	121.5	0.89	48	/	[59]
	$(FeSiB)_{85}(FeNi_{50})_{15}$	6.015	/	157.72	1.19	31	/	[60]
	Fe-Si-B-C—Cr	/	/	146.4	/	86	17	[61]
	$Fe_{85}Si_{10}Ni_5$	/	/	254.4	1.23	/	2.25	[62]
	$Fe_{84.2}Si_{9.6}Al_{5.4}Sn_{0.8}$	/	/	119.2	/	50.4	2.85	[63]

Methodology. **R. Umetsu:** Conceptualization, Methodology. **Z.Z. Li:** Conceptualization, Methodology. **X. Tong:** Writing – review & editing. **J.T. Huo:** Writing – review & editing. **S.L. Che:** Conceptualization, Methodology, Writing – review & editing. **J.Q. Wang:** Conceptualization, Methodology, Writing – review & editing.

Declaration of Competing Interest

The authors declare that they have no known competing financial interests or personal relationships that could have appeared to influence the work reported in this paper.

Data availability

Data will be made available on request.

Acknowledgements

This work was financially supported by "Pioneer and Leading Goose" R&D Program of Zhejiang (2022C01023), National Natural Science Foundation of China (NSFC 52231006, 52101205, 92163108, 51922102), Science and Technology Service Network Initiative (2022T3038), and Special Foundation of Director of Ningbo Institute of Materials Technology & Engineering (E30101QF01). This work was also partially supported by the joint project with TIZ Advanced Alloy Technology Co., Ltd. (NIMTE-51-2021-13).

References

[1] J.M. Silveyra, E. Ferrara, D.L. Huber, T.C. Monson, Soft magnetic materials for a sustainable and electrified world, Science 362 (2018) eaao0195.
[2] Z.-.H. Li, S.-.K. Xie, G.-.D. Wang, H.-.T. Liu, Ultrathin-gauge high silicon non-oriented electrical steel with high permeability and low core loss fabricated by optimized two-stage cold rolling method, Mater. Charact. 183 (2022), 111593.
[3] B. Zhang, Y. Liang, S. Wen, S. Wang, X. Shi, F. Ye, J. Lin, High-strength low-iron-loss silicon steels fabricated by cold rolling, J. Magn. Magn. Mater. 474 (2019) 51–55.
[4] J. Wang, Q. Ren, Y. Luo, L. Zhang, Effect of non-metallic precipitates and grain size on core loss of non-oriented electrical silicon steels, J. Magn. Magn. Mater. 451 (2018) 454–462.
[5] Y. Guo, D. Ma, X. Li, L. Lu, Y. Gao, Y. Shen, T. Zhang, Effects of room temperature rolling in different directions on magnetic properties, electrical properties and bending ductility of Fe85P11C2B2 amorphous alloy, J. Non Cryst. Solids 596 (2022), 121875.
[6] A. Krings, A. Boglietti, A. Cavagnino, S. Sprague, Soft magnetic material status and trends in electric machines, IEEE Trans. Ind. Electron. 64 (2017) 2405–2414.
[7] S. Dobák, P. Kollár, J. Füzer, R. Bureš, M. Fáberová, On the ferrite-controlled iron coupling for enhanced soft magnetic hybrid composites via first-order reversal curves, Acta Mater. 246 (2023), 118667.
[8] N.M. Bruno, N.A. Adoo, E. Meakins, V. Keylin, G.E. Feichter, R.D. Noebe, The effect of stress-annealing on the mechanical and magnetic properties of several Fe-based metal-amorphous nano-composite soft magnetic alloys, J. Non Cryst. Solids 600 (2023), 122037.
[9] G. Herzer, Modern soft magnets: amorphous and nanocrystalline materials, Acta Mater. 61 (2013) 718–734.
[10] Y. Huang, B. Zang, C. Zhang, M. Xiang, P. Xiao, J. Huo, M. Gao, R. Umetsu, M. Ji, B. Yao, Y. Zhang, Y. Wang, J. Wang, Polydopamine/polyethyleneimine enhanced Fe-based amorphous powder cores with improved magnetic properties, J. Alloys Compd. 920 (2022), 165889.
[11] X. Wu, B. Tang, Q. Wang, Y. Wu, D. Li, D. Ding, X. Guo, L. Xia, P. Yu, Modulation of soft magnetic properties of Fe83B10P4C2Cu1 amorphous alloys by V addition and annealing treatment, J. Non Cryst. Solids 602 (2023), 122096.
[12] G. Zhang, H. Ni, Y. Li, T. Liu, A. Wang, H. Zhang, Fe-based amorphous alloys with superior soft-magnetic properties prepared via smelting reduction of high-phosphorus oolitic iron ore, Intermetallics 141 (2022), 107441.
[13] F.C. Li, T. Liu, J.Y. Zhang, S. Shuang, Q. Wang, A.D. Wang, J.G. Wang, Y. Yang, Amorphous–nanocrystalline alloys: fabrication, properties, and applications, Mater. Today Adv. 4 (2019), 100027.
[14] H. Zhang, Y. Wu, J. Zeng, T. Liu, S. Mo, H. Ni, Calculation assisted composition design of Fe-based amorphous alloys, J. Non Cryst. Solids 600 (2023), 122011.
[15] W.H. Wang, C. Dong, C.H. Shek, Bulk metallic glasses, Mater. Sci. Eng.: R 44 (2004) 45–89.
[16] S.J. Hong, G.H. Lee, C.K. Rhee, W.W. Kim, K.S. Lee, Magnetic pulsed compaction of ferromagnetic nano-powders for soft-magnetic core, Mater. Sci. Eng.: A 449-451 (2007) 401–406.
[17] H. Shokrollahi, K. Janghorban, Soft magnetic composite materials (SMCs), J. Mater. Process. Technol. 189 (2007) 1–12.
[18] J.M. Silveyra, E. Ferrara, D.L. Huber, T.C. Monson, Soft magnetic materials for a sustainable and electrified world, Science 362 (2018) 418.
[19] X. Li, A. Makino, H. Kato, A. Inoue, T. Kubota, Fe76Si9.6B8.4P6 glassy powder soft-magnetic cores with low core loss prepared by spark-plasma sintering, Mater. Sci. Eng.: B 176 (2011) 1247–1250.
[20] X.-y. Wang, Z.-c. Lu, C.-w. Lu, G.-m. Li, D.-r. Li, Magnetic properties of FeSiBC amorphous alloy powder cores using mechanical-crushed powder, J. Iron Steel Res. Int. 21 (2014) 1055–1058.
[21] X. Li, Y. Wu, S. Yang, X. Cha, P. Shao, L. Wang, Preparation and degradation property of magnetic FePBCSi amorphous alloy powder, J. Non Cryst. Solids 503-504 (2019) 284–287.
[22] T. Zhao, C. Chen, X. Wu, C. Zhang, A.A. Volinsky, J. Hao, FeSiBCrC amorphous magnetic powder fabricated by gas-water combined atomization, J. Alloys Compd. 857 (2021), 157991.
[23] Y.Y. Zheng, Y.G. Wang, G.T. Xia, Amorphous soft magnetic composite-cores with various orientations of the powder-flakes, J. Magn. Magn. Mater. 396 (2015) 97–101.
[24] G. Shi, X. Hu, Y. Lai, J. Wu, M. Wang, X. Li, C. Peng, Z. Li, L. Wang, Preparation and electromagnetic performances of Finemet nanocrystalline soft magnetic composites with flake and spherical powders, J. Alloys Compd. 925 (2022), 166740.
[25] Y. Shi, W. Lu, W. Sun, S. Zhang, B. Yang, J. Wang, Impact of gas pressure on particle feature in Fe-based amorphous alloy powders via gas atomization: simulation and experiment, J. Mater. Sci. Technol. 105 (2022) 203–213.
[26] Y. Liu, Y. Yi, W. Shao, Y. Shao, Microstructure and magnetic properties of soft magnetic powder cores of amorphous and nanocrystalline alloys, J. Magn. Magn. Mater. 330 (2013) 119–133.

[27] Y.G. Nam, K.-.H. Bae, H. Kim, S. Yang, Y.-.J. Kim, J.W. Lee, J.W. Jeong, Preparation of gas-atomised amorphous soft magnetic powders with high saturated magnetisation above 1.25T realised by senary Fe73Si9−xB10P5C3Mox alloys with abnormal glass-forming ability, Powder Metall. 64 (2021) 173–179.
[28] T. Zhao, H. Yu, C. Sun, C. Chen, J. Hao, Effects of the substitution of Si with P on the glass forming ability, crystallization behavior, and magnetic properties of FeCuNbSiBP atomized powder, J. Magn. Magn. Mater. 550 (2022), 169087.
[29] H. Huang, R. Zhang, H. Sun, J. Zhang, J. Wang, High density Fe-based soft magnetic composites with nice magnetic properties prepared by warm compaction, J. Alloys Compd. 947 (2023), 169460.
[30] B.V. Neamţu, T.F. Marinca, I. Chicinaş, O. Isnard, F. Popa, P. Păşcuţă, Preparation and soft magnetic properties of spark plasma sintered compacts based on Fe–Si–B glassy powder, J. Alloys Compd. 600 (2014) 1–7.
[31] A. Singh, S.P. Harimkar, Spark plasma sintering of in situ and ex situ iron-based amorphous matrix composites, J. Alloys Compd. 497 (2010) 121–126.
[32] S.B. Yarusova, O.O. Shichalin, A.A. Belov, S.A. Azon, I.Y. Buravlev, A.V. Golub, V. Y. Mayorov, A.V. Gerasimenko, E.K. Papynov, A.I. Ivanets, A.A. Buravleva, E. B. Merkulov, V.A. Nepomnyushchaya, O.V. Kapustina, P.S. Gordienko, Synthesis of amorphous KAlSi3O8 for cesium radionuclide immobilization into solid matrices using spark plasma sintering technique, Ceram. Int. 48 (2022) 3808–3817.
[33] X.C. Zhong, S.M. Wu, X.T. Dong, Y.X. Li, J.H. Huang, C.L. Liu, H. Zhang, Y. L. Huang, H.Y. Yu, W.Q. Qiu, Z.W. Liu, M.L. Zhong, Z.C. Zhong, R.V. Ramanujan, High density La-Fe-Si based magnetocaloric composites with excellent properties produced by spark plasma sintering, Mater. Sci. Eng.: B 280 (2022), 115717.
[34] L. Yanmaz, F.C. Sahin, Investigation of the density and microstructure homogeneity of square-shaped B4C-ZrB2 composites produced by spark plasma sintering method, J. Eur. Ceram. Soc. 43 (2023) 1295–1302.
[35] C. Zhao, A. Wang, A. He, C. Chang, C.-.T. Liu, Nano-heterogeneity-stabilized and magnetic-interaction-modulated metallic glasses, Sci. China Mater. 64 (2021) 1813–1819.
[36] H.R. Lashgari, D. Chu, S. Xie, H. Sun, M. Ferry, S. Li, Composition dependence of the microstructure and soft magnetic properties of Fe-based amorphous/nanocrystalline alloys: a review study, J. Non Cryst. Solids 391 (2014) 61–82.
[37] Y. Meng, S. Pang, C. Chang, J. Luan, A. Inoue, T. Zhang, Effects of Si on the microstructure, soft magnetic properties and bendability of rapidly-annealed nanocrystalline Fe–Si–B–P–Cu alloy ribbons, J. Alloys Compd. 940 (2023), 168799.
[38] X. Fan, T. Zhang, W. Yang, J. Luan, Z. Jiao, H. Li, Design of FeSiBPCu soft magnetic alloys with good amorphous forming ability and ultra-wide crystallization window, J. Mater. Sci. Technol. 147 (2023) 124–131.
[39] Z.W. Liu, H.Y. Huang, X.X. Gao, H.Y. Yu, X.C. Zhong, J. Zhu, D.C. Zeng, Microstructure and property evolution of isotropic and anisotropic NdFeB magnets fabricated from nanocrystalline ribbons by spark plasma sintering and hot deformation, J. Phys. D 44 (2011), 025003.
[40] T. Liu, F. Li, A. Wang, L. Xie, Q. He, J. Luan, A. He, X. Wang, C.T. Liu, Y. Yang, High performance Fe-based nanocrystalline alloys with excellent thermal stability, J. Alloys Compd. 776 (2019) 606–613.
[41] Y.L. Li, Z.X. Dou, X.M. Chen, K. Lv, F.S. Li, X.D. Hui, Improving the amorphous forming ability and magnetic properties of FeSiBPCu amorphous and nanocrystalline alloys by utilizing carbon, J. Alloys Compd. 844 (2020), 155767.
[42] X. Fan, M. Jiang, T. Zhang, L. Hou, C. Wang, B. Shen, Thermal, structural and soft magnetic properties of FeSiBPCCu alloys, J. Non Cryst. Solids 533 (2020), 119941.
[43] J. Schroers, Processing of Bulk Metallic Glass, Adv. Mater. 22 (2010) 1566–1597.
[44] Y. Kodera, T. Yamamoto, N. Toyofuku, M. Ohyanagi, Z.A. Munir, Role of disorder-order transformation in consolidation of ceramics, J. Mater. Sci. 41 (2006) 727–732.
[45] Z. Xiao, C. Tang, H. Zhao, D. Zhang, Y. Li, Effects of sintering temperature on microstructure and property evolution of Fe81Cu2Nb3Si14 soft magnetic materials fabricated from amorphous melt-spun ribbons by spark plasma sintering technique, J. Non Cryst. Solids 358 (2012) 114–118.
[46] M. Ohta, Y. Yoshizawa, Recent progress in high Bs Fe-based nanocrystalline soft magnetic alloys, J. Phys. D 44 (2011), 064004.
[47] G. Herzer, Grain structure and magnetism of nanocrystalline ferromagnets, IEEE Trans. Magn. 25 (1989) 3327–3329.
[48] G. Herzer, Grain size dependence of coercivity and permeability in nanocrystalline ferromagnets, IEEE Trans. Magn. 26 (1990) 1397–1402.
[49] Y. Zhang, P. Sharma, A. Makino, Fe-Rich Fe–Si–B–P–Cu powder cores for high-frequency power electronic applications, IEEE Trans. Magn. 50 (2014) 1–4.
[50] K. Geng, Y. Xie, L. Yan, B. Yan, Fe-Si/ZrO2 composites with core-shell structure and excellent magnetic properties prepared by mechanical milling and spark plasma sintering, J. Alloys Compd. 718 (2017) 53–62.
[51] T. Larimian, V. Chaudhary, J. Christudasjustus, R.V. Ramanujan, R. Gupta, T. Borkar, Bulk-nano spark plasma sintered Fe-Si-B-Cu-Nb based magnetic alloys, Intermetallics 124 (2020), 106869.
[52] Y. Zhang, P. Sharma, A. Makino, Sintered powder cores of high Bs and low coreloss Fe84.3Si4B8P3Cu0.7 nano-crystalline alloy, AIP Adv. 3 (2013), 062118.
[53] M. Tian, J. Xu, S. Yang, J. Wang, T. Yang, G. Li, Q. Chen, X. Liu, Effects of heat treatment and compaction pressure on the microstructure and magnetic properties of core-shell structured FeSiBNbCu/SiO2 soft magnetic composites, J. Alloys Compd. 923 (2022), 166394.
[54] X. Li, Y. Dong, X. Liu, S. Wu, R. Zhao, H. Wu, W. Gao, A. He, J. Li, X. Wang, Structure evolution of Fe-based nanocrystalline soft magnetic powder cores with excellent properties, Mater. Sci. Eng. B 285 (2022), 115965.
[55] H. Wei, H. Yu, Y. Feng, Y. Wang, J. He, Z. Liu, High permeability and low core loss nanocrystalline soft magnetic composites based on FeSiBNbCu@Fe3O4 powders prepared by HNO3 oxidation, Mater. Chem. Phys. 263 (2021), 124427.
[56] B. Zhou, Y. Dong, L. Liu, L. Chang, F. Bi, X. Wang, Enhanced soft magnetic properties of the Fe-based amorphous powder cores with novel TiO2 insulation coating layer, J. Magn. Magn. Mater. 474 (2019) 1–8.
[57] L. Chang, L. Xie, M. Liu, Q. Li, Y. Dong, C. Chang, X.-.M. Wang, A. Inoue, Novel Fe-based nanocrystalline powder cores with excellent magnetic properties produced using gas-atomized powder, J. Magn. Magn. Mater. 452 (2018) 442–446.
[58] C. Wu, H. Chen, H. Lv, M. Yan, Interplay of crystallization, stress relaxation and magnetic properties for FeCuNbSiB soft magnetic composites, J. Alloys Compd. 673 (2016) 278–282.
[59] Y. Zhang, Y. Dong, B. Zhou, Q. Chi, L. Chang, M. Gong, J. Huang, Y. Pan, A. He, J. Li, X. Wang, Poly-para-xylylene enhanced Fe-based amorphous powder cores with improved soft magnetic properties via chemical vapor deposition, Mater. Des. 191 (2020), 108650.
[60] B. Li, Z.G. Zheng, H.Y. Yu, D.C. Zeng, Improved permeability of Fe based amorphous magnetic powder cores by adding Permalloy, J. Magn. Magn. Mater. 438 (2017) 138–143.
[61] B. Zhou, Y. Dong, L. Liu, Q. Chi, Y. Zhang, L. Chang, F. Bi, X. Wang, The core-shell structured Fe-based amorphous magnetic powder cores with excellent magnetic properties, Adv. Powder Technol. 30 (2019) 1504–1512.
[62] W. Xu, C. Wu, M. Yan, Preparation of Fe–Si–Ni soft magnetic composites with excellent high-frequency properties, J. Magn. Magn. Mater. 381 (2015) 116–119.
[63] Z. Liu, Y. Dong, X. Liu, H. Lu, Y. Wu, R. Zhang, Y. Ma, H. Zhang, X. Jia, A. He, J. Li, X. Wang, Optimizing soft magnetic properties by reducing internal defects and residual stress of Fe85-xSi9.6Al5.4Snx soft magnetic composites, J. Mater. Res. Technol. 18 (2022) 3872–3883.